Developing a FRET tension sensor-compatible system for analyzing cardiomyocyte tension alongside applied strain

CHERRY LEUNG

A thesis

submitted in partial fulfillment of the

requirements for the degree of

MASTER OF SCIENCE

University of Washington

2023

Committee:

Jennifer Davis

Michael Regnier

Program Authorized to Offer Degree:

BIOENGINEERING

University of Washington

Abstract

Developing a FRET tension sensor-compatible system for analyzing cardiomyocyte tension alongside applied strain

Cherry Leung

Chair of the Supervisory Committee:
Jennifer Davis
Laboratory Medicine and Pathology, Department of Bioengineering

Cardiomyopathy refers to heart diseases in which myocardial tissue has undergone structural changes, often resulting in systolic dysfunction. Restructuring of the heart is influenced by mechanical forces and these organ-level changes are reflected by remodeling at the cellular level as well. Sarcomeres are the basic contractile unit of muscle tissues, and the direction in which they are added influences the shape of the cells and consequently the shape of the overall heart. Many existing cardiomyopathy therapies only address disease symptoms, such as reducing blood pressure with beta-blockers, but do not solve the underlying issue of systolic dysfunction. Current research focuses on genetic or biochemical methods, whereas manipulating the mechanics would allow for intervention upstream of those targets. Since mechanical forces such as tension strongly influence the development of various phenotypes, an alternative approach would be to leverage these mechanical interactions in the heart to specifically target cell remodeling. However, our current understanding of the relationship between tension and cellular remodeling is incomplete. Recent developments in the field have allowed for FRET force sensors to measure intracellular tension at focal adhesions, but are limited when it comes to externally applied forces. The goal of this project is to design a system capable of measuring intracellular tensile forces when applying an external strain, comprised of two parts. First, by culturing cardiomyocytes derived from a cell line expressing a FRET sensor line on a flexible substrate, it will be possible to image active tension forces experienced in the cell by applying a uniaxial strain. Secondly, the development of a free-standing cardiomyocyte monolayer "cell sheet" would allow for tension imaging of stretched cardiomyocytes alone without a support membrane. The system should allow for the study of how cells sense tension when an external force is applied and in what capacity.

Introduction

Heart Disease and Remodeling

The heart can scar or remodel when injured or put under stress, which leads to changes in its geometry [1]. However, even in healthy hearts, cells regularly experience strain and tensile forces as the heart beats and the cells contract. During the systolic portion of a cardiac cycle, blood fills the left ventricle of the heart and stretches the cardiomyocytes. This stretching force is referred to as preload and depends on the venous return, which is controlled by the pressure and volume of the blood. This can increase due to physical factors such as exercise or neurohormones [2]. In response to exercise, myosin isoforms may switch to change the speed of force generation and the number of contractile units in the cell increases [3]. When exposed to increased afterload and wall stress, which can happen during exercise, sarcomeres will add in parallel causing thickened, hypertrophied tissue. Overstretching will cause sarcomeres to be added in series and lengthen the tissue.

Other factors contributing to heart disease include chronic hypertrophy or oxidative stress. Chronic hypertrophy is linked to fibrosis and apoptosis while oxidative stress can trigger hypertrophic signaling cascades and directly decrease contractile force and relaxation. After myocardial infarction (MI), cells also rearrange across the ventricular wall to compensate for the dead cells and are at a higher risk of distension and deformation. Cardiac remodeling is also associated with conditions such as arrhythmia, contractile dysfunction, loss of ventricular function, and heart failure [4], [5]. For example, in hypertrophic cardiomyopathy (HCM) the walls of the left ventricle thicken and become stiff. This leads to a reduction in the overall volume in the heart chamber which forces the heart to work harder to achieve the same output as before. HCM is commonly associated with diastolic dysfunction and an increased risk of sudden cardiac death [6].

Cellular Contraction and Adhesion Structures

Muscle fibers are comprised of myofibrils that are made up of stacked contractile units called the sarcomere (**Fig. 1A**). The length of a sarcomere is measured from z-line to z-line and consists of thin filaments made up of actin and thick filaments made up of myosin. During contraction, proteins on the actin filaments called troponin bind to calcium and expose myosin binding sites. The myosin heads on the thick filament are then able to bind and slide along the thin filaments, causing contraction and bringing the z-lines closer together. During preload, cardiomyocytes are stretched and the sarcomeres lengthen. The myofibrils have an increased sensitivity to calcium which causes the sarcomere to contract with greater force [7]. This property of cardiac cells where increased preload results in increased contractility are referred to as the Frank-Starling mechanism.

Cells have mechanosensors to sense force in their environment. These mechanosensors are fixed to structures such as the extracellular matrix (ECM), cytoskeleton, or within lipid

bilayers [8]. Conformational changes of these mechanosensors are translated into biochemical signaling pathways through proteins or enzyme interactions. Integrins are proteins on the cell surface that connect to the ECM [5]. Focal adhesions are transmembrane protein complexes that mechanically link the cell to the ECM and include a mechanosensitive protein called vinculin that responds to changes in tension across the focal adhesion [9], [10]. Vinculin is bound to actin filaments that then connect to sarcomeres (**Fig. 1B**).

Cellular Remodeling

In studying cardiovascular diseases such as cardiomyopathy, researchers noticed that mechanical forces caused the cell to pathologically remodel and become hypertrophic [2], [11]. The heart will hypertrophy as a compensatory mechanism to accommodate for the increased preload. Different forms of hypertrophic remodeling in cells have different patterns of sarcomere addition [1]. For example, volume overload leads to eccentric hypertrophy where the left ventricle volume increases but the wall thickness remains the same. Pressure overload stress leads to concentric hypertrophy where the ventricle volume remains relatively constant but the wall thickness increases. Davis et. al has also shown that an increased integral of tension over time is a predictor of concentric remodeling and a decrease in the tension integral is correlated with eccentric hypertrophy [12].

Long-term effects of hemodynamic overload can lead to pathological remodeling resulting in cardiac dysfunction [5]. For instance, maladaptive remodeling after MI has sarcomeres being added in series. This causes the cardiomyocytes to have decreased force output and leads to contractile dysfunction, ventricular dilation, and arrhythmia [4],[5]. Cardiomyocytes can also sense the stiffness of the environment and may hypertrophy in response through a signaling pathway in which vinculin is recruited by another cytoskeletal protein [11]. The elasticity and stiffness of the culture substrate can impact cytoskeletal structures within the cell and impact the contractile forces as well [13].

It is shown that sarcomeres grow under high tensile stress, which is related to mechanical tension [2], [14]. The mechanical stress in the ventricular walls activates hypertrophic signaling pathways in the cells through mechanosensitive ion channels and integrins. This correlation between the cell's tensile stress, sarcomere growth, and pathological remodeling of the cardiomyocyte inspires further research into understanding how exactly the forces affect cell behavior or how mutations result in different disease phenotypes [14], [15]. It is unknown how the cells are able to sense the strain in their environment or how the forces affect the long-term structures of the cells.

In Vitro Myocyte Stretching and Applications

In vitro stretching experiments typically have applications in differentiating stem cells into cardiomyocytes, in which applied strain can impact the orientation of cells as well as the organization of sarcomeres [13]. Dynamic stretching tends to have more success than static

stretches in this regard, and most employ a cyclic strain between 5-15% to emulate physiological conditions. Other experiments delve into using stretch to identify specific molecules, proteins, or signaling pathways activated in response to mechanical stimuli. Much of the literature around cell stretching imaging focuses on developing devices to image adherent cells, often on a PDMS hydrogel backing, or focuses on mechanical stretching to develop functional tissues and mature cells [16]–[19]. In the field of tissue engineering and regenerative medicine, cellular stretching has also been used as part of a "cardiac patch" containing progenitor cells wherein its application to heart tissue after induced MI resulted in replacement of the damaged tissue and restoring ventricular output [13].

Technological Gap and Engineering Need

Classic mechanics measurements rely on using sarcomere length to determine cell contractility. The standard for visualizing sarcomeres alongside tension was to use antibodies to stain for the z-lines after fixing the cells in paraformaldehyde, a process that kills the cells. The sarcomeric protein used to visualize the z-lines is α-actinin (**Fig. 1A**). Current technology is incompatible with live-cell imaging of both cellular tension and sarcomeres due to spectral interference with the current tools used to measure cell adhesion tension. Instead of using a stain, if we intrinsically add a fluorophore to α-actinin to create a fusion protein, it is possible to visualize sarcomeres using live fluorescent microscopy techniques.

Additionally, it is important to understand how the focal adhesion tension changes when cardiomyocytes are stretched. There exist several different methods to measure cellular forces, including optical or magnetic tweezers, atomic force microscopy (AFM), and traction force microscopy (TFM). Optical and magnetic tweezers have a range of motion limited to about 400 nm and 50 nm respectively, however cardiomyocytes are on a much larger scale at around 100 μm in size [20]. AFM and TFM methods lack compatibility with devices that can apply an external force. Instead, the method of interest for this project lies in Förster resonance energy transfer (FRET) based biosensors. A number of FRET sensors have been developed and used primarily to study molecular tension, with recent advancements allowing for the study of intracellular tension at focal adhesions [21].

Though there have been many experiments characterizing the effects of cell stretching and its uses, there have not been any studies that correlate the intracellular force readout in relation to a known applied force. To answer this, we must be able to measure cellular force as cells are being stretched. Our approach to this was to culture cells on a flexible surface compatible with an externally applied stretch and measure the cellular force using the VinTS construct. This method stretches the substrate itself, and the strain is transferred to the cells through the cellular attachments where the cell adheres to the substrate.

Mechanical rigs are also often used to measure cellular force. Typically, they consist of a length controller that is used to stretch the tissue of interest and a stationary force transducer on the other end. There are no single-cell mechanical rigs for studying focal adhesion tension, as that would require placing the length controller and force transducer directly on the cell's

membrane, which is where the focal adhesions are located (**Fig. 2**). Alternatively, if we were to use a multicellular structure we would then be able to place the length controller and force transducer on either end of the tissue and analyze the tension in many of the cell-cell contacts in between the two attachments.

Being able to culture a free-standing monolayer of cardiac cells that is strong enough to be stretched without a backing membrane would allow us to determine the tension force directly experienced by the cells. Traditional methods of creating a monolayer use adherent cell culture methods rather than suspension techniques due to the formation of cell aggregates. One of the drawbacks to adherent culture techniques is that the enzymes used to detach the cells are harsh and destroy the ECM and thus cell-cell contacts. Alternatively, the use of thermosensitive surfaces that allow cells to lift off intact may be applied here. This method avoids using traditional enzymatic dissociation reagents and thus preserves cell-cell junctions and the ECM, which makes this technology favored by many in the cell sheet engineering field [22]. Applications of cell sheet engineering are predominantly geared toward regenerative medicine or tissue engineering purposes.

Here, we aim to investigate the specific forces experienced by the cell under an externally applied strain by developing and adapting two platforms. First, by culturing cardiomyocytes on a flexible substrate, it will be possible to investigate tension forces experienced in the cell by applying a uniaxial cyclic strain using live-cell imaging. Secondly, the development of a stretchable, free-standing cardiomyocyte monolayer "cell sheet" would allow for analyzing the intracellular tension in stretched myocytes alone without a support membrane. These systems will be used in conjunction with high-resolution multi-channel fluorescent imaging to visualize subcellular structures, allowing for the study of changes in cellular tension as a function of cellular strain.

Materials & Approach

Vinculin Tension Sensor Cell Line

The Vinculin Tension Sensor (VinTS) line was developed by Nagle in the Davis lab through the modification of a WTC11 line to heterozygously express a tension sensor. The WTC11 human induced pluripotent stem cell (hiPSC) line is the model most commonly used for studying cardiomyopathy. The Clover-mRuby2 fluorophore pair was knocked in at the native vinculin locus, with Clover being expressed at the head of the vinculin protein and mRuby2 on the tail (**Fig. 1B**). The red-green fluorophores mRuby2 and Clover were chosen due to their improved dynamic range and FRET interactions over other existing FRET pairs [23]. Sensitized emission occurs when the cells are in a relaxed state and the vinculin head and tail are in close proximity. The emission spectra of the Clover fluorophore overlap with the mRuby2 excitation spectra, which would allow emissions from the green "sensitizer" fluorophore to excite the red "emitter" fluorophore when the fluorophores are physically close together (**Fig. 3**).

If the cell is under tension, the vinculin domains would have a greater distance between them and the FRET efficiency would decrease. Given information about the distance, we can determine the force experienced by vinculin because the two fluorophores are physically connected by a linker. Since we know the stiffness of the linker, we therefore know the force that is used to keep the two fluorophores apart. This allows us to use the FRET efficiency to relay information about the distance between the fluorophores, which can then be used to determine the force experienced by vinculin.

Designing the Blue Fluorescent Protein-Tagged α-Actinin Plasmid

One critical aspect of designing the fluorophore-tagged α-actinin plasmid is that the fluorophore chosen for the sarcomeres must have excitation and emission spectra distinct enough from the existing fluorophores. This is to avoid overlapping the signals beyond what is necessary. Ideally, the transfected cells will have high expression levels only at α-actinin or have minimal off-target expression. One technical limitation is that the fluorophores used must also be in ranges that are compatible with our current microscopes, which include the blue, green, red, and far-red channels. There are only a finite number of fluorescent proteins that we have discovered and have a limited wavelength range that we can utilize.

Within the plasmid genome, we must also consider certain features of the coding sequence. It is common to add an antibiotic resistance gene to increase transformation efficiency when introducing the plasmid to bacteria and growing on an antibiotic agar plate. There are also features that initiate translation. One example is the vertebrate Kozak sequence, and in human cells, we need a promoter and enhancer sequence that are not species nor cell-specific to ensure our genes can be expressed in any of the cells we use. Thus, we chose to use the CMV promoter and enhancer which is expressed in all human cell types. Additionally, the poly-A tail improves the stability of mRNA molecules and prevents degradation, making it an important feature for gene expression [24].

We must also consider the mRNA and protein-level structures that come from the DNA sequence, which can impact expression or efficiency levels. Physical constraints such as steric hindrance between two proteins placed in proximity could be mitigated by including several amino acids in between these two genes to allow for flexibility.

Given these constraints, we elected to use EBFP2, a blue fluorescent protein (BFP) gene, and the pUC19 plasmid, which already has ampicillin resistance in addition to including basic machinery that allows the plasmid to self-replicate, such as the origin of replication. The excitation and emission spectra of the BFP do not interfere with Clover or mRuby2, which allows this construct to be used alongside cells expressing the VinTS when imaging cellular tension (**Fig. 3**). Our chosen BFP is excited by a higher energy wavelength and is more toxic to cells, which may impact the efficacy of live-cell imaging. If possible, we would utilize a far-red protein closer to the infrared range which is lower energy, however many of the existing genetically encodable proteins in that wavelength either also overlap with the red wavelengths and are not suitable for this purpose.

Cloning the BFP-Tagged α-Actinin Plasmid

To build this plasmid, the EBFP2 gene was packaged into the pUC19 plasmid containing an ampicillin resistance gene. The pUC19 backbone was first digested with both HindII and SalI restriction enzymes and the BFP insert was amplified during PCR. The BFP insert also includes a CMV promoter and CMV enhancer. Next, the BFP product was isolated by gel electrophoresis and DNA purification. The purified DNA should now have homology to the pUC19 backbone due to the primers used during the PCR amplification step. Once bacterial colonies had grown, a screening method called colony PCR was performed in which certain clones of the colony were sampled and run through a PCR using the same primers as before, which should amplify the insert if it was present in the clone. The colony PCR product was then run on a gel to identify if the samples had a band the same size as the insert. From there, the colonies that had the clearest or strongest bands were sequenced again, selecting the clone that had the best sequencing result or the least amount of mutations to proceed. This clone was used as the new intermediate vector and the primer design and assembly process was repeated for the second insert (α-actinin with a poly-A tail) using a new restriction enzyme site. After checking the band size with the gel and PCR, the best clones were once again chosen to sequence to determine which clone had the best integration of the insert.

Once the plasmid containing the fusion protein had been successfully constructed, the next step was to transfect the engineered plasmid into cells to ensure the fusion protein was expressed properly. Both WTC11 and HEK293T cell lines were used. Initial transfections using GeneJuice (Sigma-Aldrich) required an optimization step. This entailed varying the amount of transfection reagent (µL of GeneJuice) to the amount of DNA (µg plasmid) within the ranges suggested by the manufacturer. To check that the fluorophore functioned correctly and to identify which conditions yielded the best results, the transfected cells were imaged under a widefield microscope and checked for the percentage of cells expressing the BFP on the sarcomere z-lines versus the total number of cells in the image. From the different ratios, the condition with the highest transfection efficiency was chosen for future transfections. Additional plasmids were made to prepare the plasmid for lentiviral and adenoviral packaging based on a pRRL and pShuttle map respectively.

Imaging Setup

The Leica SP8 Confocal Microscope is capable of multichannel imaging at high resolution. It can be used alongside the ibidi Stage Top incubator system for live-cell imaging atop a multiwell plate holder [25]. The Nikon Live-Cell Widefield System has an enclosed chamber making it suitable for long-term live-cell imaging and is also equipped with a Spinning Disk Confocal Microscope that has lasers for exciting blue, green, red, and far-red fluorophores. The settings for excitation wavelengths and emission collection ranges differed slightly depending on the microscopes (**Fig. 4**). The Leica Confocal has more customizability around selecting the wavelength range for collecting emissions in bins, whereas the Nikon Spinning Disk collection range is predetermined by the filter cubes used.

The Cytostretcher-LV (CuriBio) is a stage-mountable device designed for live-cell imaging while applying cyclic uniaxial strain [26]. The device is operated by the NanoSurface Operational Mechanics Interface (NaOMI) software (CuriBio) and allows the user to specify the type of stretch. NaOMI grants control over the speed, distance, duration, and waveform of the stretch protocol. Once the protocol is sent to the device and started, one of the posts will move to the set distance, stretching the flexible chamber. The stretching can be imaged at any point in time. This device is compatible with live-cell imaging on the Nikon Spinning Disk Confocal Microscope, but not the Leica SP8 Confocal due to the imaging chamber of the Cytostretcher-LV being larger than the ibidi Stage Top Incubator lid attachment.

Mandrycky and Mohran in the Mack and Reginer labs have developed two mechanical rigs capable of stretching tissues and intracellular structures. Their myofibril rig can be used to measure tension in cultured tissue by affixing the tissue of interest to a stationary force transducer on one end and a mobile glass capillary tube on the other to apply unidirectional strain using hydraulics. The glass capillary tubes were previously calibrated in order to correlate the visual deflection in the tube with applied force. This is set atop a fluorescent microscope and can measure tensile force as a function of increased stretch. In the past, this myofibril rig has been primarily used to image myofibrils but has also been used to image stretched EHTs with fluorescent data alongside force data. The intact rig is also suited for force measurements and has been used to measure contractile force in strips of muscle tissues. It has two prongs, one used to control deflection and the other is a stationary prong acting as the force sensor. Tissues are clamped on either end with T-clips, which have a hole in the body to allow the tissue to be placed onto the two prongs and stretched.

Cultureware

Commercially available temperature-responsive cell culture surfaces are grafted with the thermoresponsive polymer poly(N-isopropylacrylamide) (PIPAAm). Thermo Scientific™ offers Nunc™ UpCell™ plates, which come in a variety of well counts, all coated with PIPAAm [27]. Plates coated with PIPAAm are hydrophobic at 37°C and become hydrophilic at 25°C, which allows cells to detach from the cultureware surface at room temperature. For this project, the 12-well plates were used to culture cell sheets.

CuriBio offers a variety of well sizes and orientations, though only a subset is compatible with the Cytostretcher-LV. These optically transparent flexible elastomers can also be nanopatterned with grooves either parallel or orthogonal to the direction of stretch. For this project, only the unpatterned, medium chamber was used. The medium well size measures 12 mm by 12 mm and up to one chamber fits on the Cytostretcher-LV at a time [28].

Quick Curing Tissue-Compatible Adhesives

The myofibril rig has glass capillary tubes connected to force transducers that make contact with the tissue as it rests in a well of media. To attach the cell sheets to the glass tubes, we needed a substance that could be applied while wet, solidify quickly, and stick to tissues.

Many adhesives use UV to cure quickly, but often do not bond when wet or are otherwise incompatible with tissues. Gelatin Methacrylate (GelMA) is a biomaterial that is used often in a variety of tissue engineering applications, so we chose to use GelMA with a UV photoinitiator to create a hydrogel that we could use as an adhesive. The PhotoGel®-IRG Methacrylated Gelatin Kit was purchased from Advanced Biomatrix and made up immediately prior to usage [29]. Since the hydrogel is not a pre-made solution, we have the ability to adjust the stiffness of the hydrogel to match the stiffness of the cell sheets by changing the amount of GelMA or crosslinker used when preparing the solution.

Results

Culturing and Imaging VinTS Cardiomyocytes on Cytostretcher Chamber Wells

Cytostretcher wells were seeded with induced pluripotent stem cell-derived cardiomyocytes (iPSC-CMs) from the VinTS cell line at two densities. The higher density of 620k cells/mL was used to analyze the tension in cells that are part of a colony, and the sparser 62k/mL density was for analyzing individual cells (**Fig. 5A,B**). We also performed a lipofectamine transfection on a batch of two wells in order to introduce the engineered BFP α-actinin fusion protein plasmid construct into the iPSC-CMs. This would allow us to correlate the FRET efficiency readout to actual cell contractility by measuring the changes in sarcomere length. However, the two wells used were seeded sparsely and had lots of cell death, and thus we were unable to locate a cell that had clear integration of the BFP in the sarcomere structure as opposed to autofluorescence.

These Cytostretcher chamber wells were imaged atop the Nikon Live-Cell Spinning Disk Confocal microscope using the Cytostretcher-LV stage top attachment. Along the axis of stretch, cells at varying positions through the chamber were identified and imaged. These positions were named “close” for cells near the edge of the chamber well closest to the stationary rod, “middle” for cells in the center of the chamber well, and “three-quarters” for the cells midway between the center of the chamber and the far end of the chamber that is close to the moving rod. At each location, the cells were imaged during the relaxed portion of the stretching protocol and again during the stretched portion of the protocol, thus producing paired datasets. Each image captured signal for Clover, mRuby2, and sensitized emission, as well as for the BFP for the sets that were transfected. The hold times in the protocol provided sufficient time for multichannel still images. Unfortunately, the microscope’s slow speed of filter cube switching prevented the simultaneous capture of multichannel fluorescent movies. Instead, movies in each channel were captured sequentially to gather data on dynamic stretching. The imaging program does not allow for

changing the focus position while actively acquiring data, so any movies of dynamic stretch inevitably had cells moving out of focus and out of the field of view.

Optimization of Cell Sheet Culture Conditions

The cell sheets were initially seeded at an 800k cells/mL density onto plates coated with Matrigel for >30 mins (**Fig. 5C, D**). Seventeen days after seeding this first batch (**Table 1, Batch A**), the UpCell™ plate was moved to the tissue culture hood to begin dissociation at room temperature. Following the manufacturer's recommended harvesting method, the old media was aspirated and 50 µLs of new media was added to prevent drying out, then a PVDF membrane cut to size was applied over the top of the cells. Forceps were used to push down the membrane to maximize contact surface area with the cells while avoiding creases. After 6 minutes, the cells should have detached from the cultureware surface and attached to the membrane instead. The membrane was peeled away beginning from the edges using forceps and then transferred face-down onto a 1 mm glass cover slide. After several minutes, add a small amount of media to loosen the cells from the membrane and peel the membrane away from the glass slide. Quick examination under the microscope revealed lots of residual cells in the wells as well as on the membrane itself, and a very patchy residue of cells on the slides (**Fig. 5E,F**). These cell sheets were taken to be imaged on the Leica SP8 Confocal microscope.

Many cells were lost between the multiple transfer steps, prompting the need to devise a new harvesting method compatible with our purposes. For the next batch of cells, half of the sheets were left to dissociate at room temperature fully and the other half were tested against the membrane method as before in order to determine which was the better method (**Table 1, Batch B**). Continuing to pre-coat all wells with Matrigel and seeding at 800k cells/mL, the seeding media for two of the four wells were supplemented with 3 µg of Poly-L-Lysine (PLL) per well to improve attachment. Cells were harvested 15 days post-seeding and were left to sit at room temperature until the whole sheet was detached and free-floating in the media. At the 40-minute mark, the edges began to detach but the center remained visually unchanged. Cells continued to beat and pull at points that were still attached near the edge of the well. After approximately 1.5 hours at room temperature, the media was supplemented with 20 mM HEPES to preserve cell viability. The cell sheets were fully detached after 2 hours, and either membranes or pliers were used to pick up the sheets and manually transferred onto glass slides, adding a small amount of media to allow the sheet to unfurl and straighten out on the slide. Of the four wells, one of both conditions produced an intact sheet and both were harvested using forceps rather than the membrane. Sheets however were still stringy, small, and patchy as an 800k cells/mL density was not confluent enough. At the widest, the cell sheets measured 5.639 mm and 5.613 mm (**Fig. 6A**).

The next four wells were seeded at 1600k cells/mL density, only coated with Matrigel, and harvested at 14 days (**Table 1, Batch C**). Once the plate was set out at room temperature, the media was aspirated and replaced with new media that was supplemented with 20 mM HEPES. The edges of the sheets had detached at 30 minutes to 1 hour at room temperature. After 90

minutes, a serological pipette was used to gently pipette off the sheet. The sheet remained largely intact, though pipetting too strongly could tear a hole in the sheet. These sheets were fairly large, with their widest measuring between 7.3 mm and 8.8 mm (**Fig. 6C**). The largest sheet was very thin and dried out quickly, but the original size can still be seen in the photo.

Subsequent cultures of the cell sheets had problems with attachment to the surface. Several instances of cells not attaching properly after seeding occurred, where patches and clumps would lift off during routine feeding or washing despite being kept in a 37°C incubator where the polymer should allow for attachment (**Table 1, Batch D-F**). Other times, the cells would remain attached to the surface for several days before partially or wholly dissociating and floating freely in the media (**Table 1, Batch F-H**). The addition of ECM proteins such as PLL or laminin into the seeding media did not improve attachment rates (**Table 1, Batch D,G-H**), nor did an increased incubation time for Matrigel pre-coating (**Table 1, Batch G**).

We decided to add fibroblasts when seeding the sheets to confer structural support (**Table 1, Batch E-H**). This came in the form of either HS27A cells, a fibroblast cell line, or unpurified differentiated cells that naturally include stromal cells within the population. A total of four wells were seeded confluently at 1600k/mL density (**Table 1, Batch E,F**), with two of the wells having been coated with Matrigel previously but were unused and aspirated (**Table 1, Batch E**). The two wells from Batch E did not survive.

The last two batches of sheets were harvested on the same day for imaging on the mechanical rigs. Only the sheets from Batch G ended up being used, and Batch H was preserved for size measurements. This sheet measured 9.967 mm by 7.423 mm (**Fig. 6D**).

Imaging Cell Sheets on Mechanical Rigs

During preliminary tests with the mechanical rigs, the tested cell sheets were able to be transferred onto the different setups and experimentally stretched. Cell sheets from Batch G and H were harvested for imaging on the two mechanical rigs (**Fig. 7**). On the myofibril rig, the fluorescent microscope has been modified to hold tissues on the microscope stage (**Fig. 7A**). To begin, we filled the well with roughly 3 mLs of feeding media before transferring a sheet from Batch G into the liquid. We initially tried using GelMA as an adhesive to attach the tissue to the glass capillary tubes. A 1 mL solution of GelMA containing 10% Igracure (1 mg of powdered Igracure total) was prepared, and around 10 μLs of the GelMA was pipetted onto the end of the glass tube. The glass tube with GelMA was pressed onto the tissue and exposed to a 365 nm UV flashlight to crosslink. After a few seconds of exposure, the GelMA remained liquid and did not harden. We tested the GelMA alone with longer exposure of up to two minutes of continuous UV exposure, and only then did it begin to solidify to some extent. An additional 1.8 mg of Igracure was dissolved in 18 μLs of MeOH and added to the remaining solution in hopes of speeding up the cure time but to no avail.

At this point, we opted to instead use superglue to adhere the tissue to the glass and began to stretch. However, the cell sheet was much larger than the intended size of tissue to be stretched on this setup, and the small capillary tubes were incompatible with stretching the sheet

to any meaningful degree. We switched to larger tubes and were able to observe that the intensity in the green fluorescent channels increased when stretch was applied. This is in line with our expectations, as when the cells are stretched the fluorophores are further away from each other and the emissions from the green fluorophore would not be absorbed by the red fluorophore. Although the system was not configured to record measurements that day, checking the fluorescence in the red channel revealed that the intensity also increased with applied strain, demonstrating the need for simultaneous capture of both channels in order to calculate the ratio between the two channels to determine FRET efficiency. Additionally, the larger tubes were not calibrated and as a result, we will not be able to determine the amount of strain that was actually being applied.

The remaining cell sheet from Batch G was stretched on the intact rig (**Fig. 7B**). Two T-clips were attached to either end of the cell sheet with the arms wrapping around the tissue and the body facing outwards. The tissue was then affixed onto the prongs to be stretched. With this setup, we know exactly how much force is being applied. However, this microscope did not inherently have fluorescent imaging capabilities and at the time of testing, we did not have access to add a fluorescent camera.

FRET Efficiency of Adherent Cells Under Applied Strain and Harvested Cell Sheets

Fluorescent channel images for the Clover, mRuby2, and sensitized emission were processed using the publicly available fret-analysis MATLAB pipeline developed by the Hoffman Lab [30]. The FRET efficiency for each image was calculated by first segmenting using ilastik to isolate the signal from the background in the mRuby2 images, and compared against the raw FRET efficiency images to calculate the mean FRET efficiency (**Fig. 8**). This process was applied for both Cytostretcher and cell sheet stretching experiments.

As a whole, the substrate-stretched cells had an average FRET efficiency of 79.57%, whereas cells in the relaxed state had an average efficiency of 79.43% (**Fig. 9A**). However, the p-value was 0.44 by a two-tailed paired t-test, indicating there is no significant difference between the two. Breaking it down by location, the FRET efficiency of the stretched vs relaxed cells at each different location was also not significantly different from each other. A 2-way ANOVA test between the FRET efficiency averages of each location (combining both stretched and relaxed cells) showed that there is no significant difference across the different locations along the chamber (**Fig. 9B**).

Fluorescent imaging of the unstretched, harvested sheets showed an average FRET efficiency of 11.3%. The dataset had a large distribution, with a standard deviation of 6.8% (**Fig. 10B**). Unfortunately, as there was only a preliminary stretching session on mechanical rigs, there is no recorded data for the cell sheet stretching experiments. The cell sheets were also transfected with the engineered BFP-tagged α-actinin plasmid, but had poor expression (**Fig. 10A**). A close-up of the Clover, mRuby2, and sensitized emission fluorescent channel images and corresponding FRET efficiency can be seen in **Figure 10C**.

Discussion

To advance our goal of understanding cellular mechanics and remodeling, there is a need for the ability to analyze cellular tension under a known applied force. To investigate the relationship between cellular strain and changes in focal adhesion tension, we devised two methods for study. First, by culturing VinTS iPSC-CMs on a flexible substrate, it will be possible to live-image active tension forces experienced in the cell under an applied uniaxial cyclic strain. Secondly, the development of a free-standing cardiomyocyte monolayer "cell sheet" would allow for tension imaging of stretched cardiomyocytes alone without a support membrane.

These platforms were used to investigate how cells sense the tension in their environment and aimed to further our understanding of how cells remodel in response to environmental forces. We were able to acquire fluorescent tension data while simultaneously applying an external, known strain to cells. The applied strain dataset acquired using Cytostretcher-LV allows us to characterize forces experienced by adherent cells under a known applied strain, and the potential for imaging of dynamic tension will contribute to our knowledge of cellular tension. We have also shown here that it is possible to culture cardiomyocyte monolayers that are strong enough to be manipulated and stretched on multiple imaging platforms while remaining intact. With the development of the cell sheet monolayers, we can take measurements on directly stretched cells, when previously cellular strain was achieved by transducing force from the stretched substrate through cellular attachments.

Cells under strain are expected to have a lower FRET efficiency as the distance between the vinculin domains would increase and therefore the distance between the fluorophores would also increase. The distance between the Cytostretcher rods measures about 21 mm, so when the chamber well is stretched an additional 1 mm, the cells should experience a 4.76% strain. Contrary to what we would expect, the results seem to indicate that cells under applied strain have no difference in FRET efficiency than cells at rest. A greater stretch distance with a physiologically relevant strain might show differences between the mean FRET efficiency and thus warrants further investigation before making a definitive conclusion.

Though the cells sheets had a much lower FRET efficiency than the relaxed cells from the Cytostretcher experiments, it is important to note that since these measurements were taken on a different microscope setup, the values are not directly comparable to those taken on the Nikon Spinning Disk as in the previous experiment. There were multiple constraints with microscope capabilities and compatibility that prevented us from acquiring a fully robust set of FRET tension data, as outlined in **Table 2**.

Limitations

Constraints of the imaging setup had significantly limited the quality of data acquired, which likely contributed to the high variability of the data. The Nikon Live-Cell Spinning Disk Confocal microscope used for imaging applied uniaxial strain was unable to achieve the resolution and speed necessary to capture the stretching dynamics. The slow speed of swapping filter cubes and the inability to change position or focus during acquisition poses significant

limitations to this method of imaging. One workaround to acquire multichannel movies was to take sequential single-channel movies in every channel, though the accuracy of the data will be highly dependent on the photostability of the fluorophores. The fluorescent channels acquisition also differs slightly from the established set of images used for FRET calculations. Namely, there is a much larger delay between images of the different channels and it is missing the green channel that is taken simultaneously with the sensitized emissions. The filter cubes also have a shorter collection range compared to the settings on the Leica SP8 Confocal and may be losing out on some signal from the fluorophores as a result. The Leica Confocal is capable of acquiring multichannel movies but is incompatible with the available live-cell imaging systems.

In addition, the z-position of the Cytostretcher chamber changes as it is stretched. The only option to keep the plane in focus is to adjust the z-plane deflection knob on the Cytostretcher-LV. However, tuning the deflection angle still could not keep the cells in focus for the full stretch cycle, due in part to the lack of fine controls. Moreover, the need for high-resolution images automatically requires a higher magnification, which naturally decreases the field of view. Cells near the stationary post would travel less horizontal distance than cells near the moving post when stretched. A set stretching distance, for example, might have cells near the moving post traversing the entire field of view during its stretch cycle, but cells near the stationary end would appear to have little to no change, thus requiring dynamic adjustment to keep the cells in the frame.

We were unable to acquire fluorescent and force data on the cell sheets. The myofibril rig was originally designed for myofibrils, which are subcellular structures much smaller than the cell sheets that were produced. The force output of the glass capillary tubes was of a much smaller magnitude than what was necessary for the cell sheets. Larger tubes were available but were not calibrated and thus would leave the force applied as an unknown factor. The resolution of the image was also poor. The intact rig can measure force through deflection, though the microscope did not have a fluorescent camera. Furthermore, due to their irregular shape, stretching the sheets will likely not result in a uniformly applied strain profile.

The cell sheets were not harvested all on the same date post-seeding. This may affect the number of established cell-cell junctions and thus produce sheets of varying strength, which has not been fully characterized. Furthermore, though the set protocol for culturing the sheets had been successful at one point, subsequent cultures failed to attach. It is unclear whether the protocol is ineffective or if the source lies in the other materials used, but the reproducibility must be improved before this method's full potential can be harnessed. The seeding density is likely too high for all the cells to adequately adhere to the surface. It would be necessary to reoptimize for different seeding densities again to determine which condition reliably yields sheets that can be manipulated to some degree without tearing.

Additionally, transfections using the BFP-tagged α-actinin plasmid had low efficiency. The BFP integration into the cell sheets tended to be weak and difficult to image. The sheets had poor signal at high magnification, with the most clarity at a magnification of either 4x or 20x. Transfection with the Cytostretcher chambers resulted in lots of cell death and ambiguous

expression. Higher magnification could potentially distinguish between actual signal versus autofluorescence, though the low total number of cells may have decreased the likelihood of seeing good expression since transfections are known to be cytotoxic.

It was also recently discovered that the VinTS cell line may be expressing a fraction of the tension sensors non-specifically, increasing the background noise levels. This decreases the signal-to-noise ratio, making it difficult to discern true force signals from nonspecific fluorescence. Though we currently have limited success with BFP expression, the de-localized VinTS issue may be mitigated by correlating fluorescent data with sarcomeric data to determine the actual amount of strain present in the cell.

Future Work

Visualization of the sarcomeres could be improved by further development of viral vectors to increase integration and expression of the engineered fusion protein plasmid. This would allow for the ability to analyze sarcomere dynamics alongside the acquired tension data. Though the fusion protein plasmid had previously been optimized, these new systems have different culturing methods and the transfection procedure must be re-optimized to preserve cell viability as well as achieve high efficiency for their specific conditions.

With the current dynamic stretching movies, segmentation of this data will require more consideration as some of the cells come in and out of focus or the field of view. One way to account for the movement of the signal would be to employ a form of particle tracking, such that only the signals that remain in focus for the entirety of the movie will be considered. The fluorescent signals that move out of the frame or out of focus should be treated as background, as including them would skew our results. The calculated FRET efficiency depends heavily on the segmentation of the frame.

Imaging of dynamic stretch may be achieved with an improved microscope setup. It may be possible to write a script that will allow the camera position to automatically follow the position of a cell during a stretch cycle while actively acquiring data. Achieving tension data as the cells are put under cyclic uniaxial strain would be highly informative. The Cytostretcher-LV allows for executing stretching protocols more complex than the one used in this project and may be possible to replicate a stretching protocol that simulates physiologically relevant conditions. Additionally, it may be beneficial to apply the same setup to chambers with nanopatterned surfaces and study how the alignment of cardiomyocytes impacts the tension in strained cells.

An alternate method for analyzing tension during stretch that is achievable with the current setup would be to take still images at different points throughout the stretch distance. Setting the NaOMI protocol to increment and hold at intervals throughout the total stretch distance will allow for the analysis of how the FRET efficiency changes with respect to the stretch distance and strain.

It is important to be imaging at the interface where the cellular attachments are in order to analyze the transduced force from substrate to cell, since a different plane may be experiencing different forces than at the attachment plane. The plane of interest was not always aligned with

the imaging plane, and in those cases, some of the signal would always be out of focus. One improvement that could be made to mitigate this effect would be to take z-stacks of the cells, which would ensure the capture of all the cellular attachments to the substrate.

With the successful development of a stretchable cardiac monolayer, the next step is to image these free-standing cell sheets to analyze the tension in the stretched sheets. This may not be able to be accomplished until the intact rig is adapted for fluorescence microscopy or another microscope setup that allows for fluorescent imaging as well as force readout is developed. These results would further illuminate the relationship between cell strain and focal adhesion tension.

Methods

Cell Culture

Cardiomyocytes were differentiated from the modified hiPSC VinTS line. The hiPSCs in mTeSR (STEMCELL) were seeded onto a 12-well plate pre-coated with Matrigel (Corning) for at least 30 minutes such that they are 50% confluent the next day. 1 μM Chiron was added to the feeding media on Day -1. For Day 0 through Day 4, the feeding media changed to RPMI 1640 (Gibco) supplemented with bovine serum albumin and ascorbic acid (RBA media). On Day 0, RBA media was supplemented with a variable amount of Chiron (3 μM, 4 μM, and 5 μM) and added to the wells in quadruplicate. On Day 2 cells were fed with RBA media with 2 μM WNTC59. Day 4 cells were fed with RBA media and Day 6 cells were fed with RPMI 1640 with B-27™ Supplement plus insulin, which is the maintenance media for cardiomyocytes. Cells were replated on Day 14 onto Matrigel-coated 12-well plates for lactate purification. On Days 16 and 18, the cells were fed with DMEM without glucose or sodium pyruvate (Gibco) and supplemented with 4 mM sodium lactate. After purification, the cells were fed on Mondays, Wednesdays, and Fridays with maintenance media until harvested for use in experiments.

HS27A cells were cultured on 10 cm plates and fed weekly with DMEM containing 10% FBS, 1% NEAA, and 1% Penicillin-Streptomycin. Cells were passaged with 5 mLs of 0.05% Trypsin about every two weeks prior to becoming confluent, using about 1% of the confluent cells when plating onto a new 10 cm plate.

Lipofectamine Transfection of Plasmid

Lipofectamine was used when transfecting the BFP-tagged α-actinin plasmid into the cardiomyocytes. For transfecting one well of the cell sheets, one solution containing 25 μLs of Opti-MEM (Gibco), 1 μg of plasmid DNA, 1 μL of P3000™ Enhancer Reagent (Invitrogen), and another solution containing 25 μLs Opti-MEM and 1 μL Lipofectamine™ 3000 Reagent (Invitrogen) were prepared and then combined. After 15 mins of incubation at room temperature, lipofectamine solution was added to 1 mL of maintenance media and added to desired well,

shaking gently for even distribution. After 1-2 hours, another 1 mL of maintenance media was added to reach the standard 2 mL/well volume. The cells were harvested to be imaged two days later. This two-day timepoint was determined to have peak expression of the construct, which was characterized in transfected hiPSCs.

Preparation of PhotoGel® Methacrylated Gelatin with Igracure

The PhotoGel kit comes with two 500 mg amber bottles of lyophilized Methacrylated Gelatin and a vial containing 100 mg of the photoinitiator Igracure. To make a 10% GelMA solution, warm 5 mLs of 1X PBS to above 60°C and add to one 500 mg bottle of the lyophilized gelatin. Mix until fully solubilized by keeping it in a 37°C rotator overnight.

Igracure in solution has a shelf life of only 2 weeks. Only add methanol to the amount of Igracure necessary, which is 1% of the volume of gelatin used. For this application, only a very small amount of GelMA will be used to crosslink the tissues to the glass capillary tubes. To create 1 mL of the hydrogel, only 0.01 mL of Igracure is necessary. Measure out 1 mg of the Igracure powder to add to 0.01 mL of methanol and mix well. Add 1 mL of the solubilized gelatin to the solution and mix thoroughly. Use a 365 mm UV light source to crosslink when ready.

Fluorescent Microscopy Settings

For the cell sheets, initial imaging was performed on a Leica SP8 Confocal microscope. The green Clover fluorophore was excited with the 488 nm laser, the red mRuby2 with 522 nm, and the blue BFP with the 405 nm laser. Individual images for each of the fluorophores present were taken by activating their respective laser and collecting in the fluorophore's emission range. Sensitized emission images were taken by activation of the 488 nm laser and collecting in both green and red channels. Brightfield images were also collected alongside these fluorescent channels.

For the Cytostretcher chambers, imaging was performed on the Nikon Live-Cell Spinning Disk Confocal Microscope with the Cytostretcher-LV mounted atop the stage. The single-channel fluorophore images and brightfield images were taken in the same manner as the cell sheets on the Leica SP8 confocal microscope. Due to the slow speed of changing filter cubes, it cannot capture both green and red channels simultaneously. Instead, to image the sensitized emission, the microscope was set to excite the Clover at 488 nm and capture the mRuby2 emission in the red channel.

Protocol for Culturing & Imaging using Cytostretcher

Sterilize the medium Cytostretcher chamber with 70% ethanol and rinse with ultrapure water (Optional: treat chambers with UV sterilization for 1 hour prior to using ethanol). Functionalize the chamber using a 90-second plasma treatment and coat immediately in 500 µLs of Matrigel. Insert short rods through the chamber and place the chamber in a sterile 60 mm or

10 cm plate to rest in the incubator for at least 30 minutes prior to seeding. Seed with 1 mL of RPMI 1640 + B27 + insulin and Rock Inhibitor containing either 620,000 or 62,000 cells. The denser seeding density amounts to about 4.31 cells/mm^2 and the sparser density is about 0.431 cells/mm^2. Allow the cells to grow for a minimum of one week prior to experimentation.

Set up the Cytostretcher-LV onto the stage of the Nikon Spinning Disk and connect the device to a computer running the NaOMI stretching software. Install the Cytostretcher chamber with rods into the slots in the Cytostretcher-LV, and run the desired protocol (**Fig. 11**). To find the focus coordinates of a given colony of cells at either the stretched or relaxed positions, run a separate "slow" protocol that gives ample time to track the position of the cells of interest through the microscope, saving the start and end coordinates as two separate points. Adjust the z-plane deflection on the Cytostretcher-LV if necessary. Run the experimental protocol with the focus set to the relaxed coordinates, taking a multi-channel image set and a movie for each fluorescent channel. Switch the focus to the stretched coordinates and repeat the stretching protocol to image the same cells, checking the readout on NaOMI to ensure that the cells are at the stretched position when relevant.

Protocol for Culturing & Imaging Cell Sheets

Coat wells in Matrigel for at least 30 mins at 37°C, using 1 mL/well for a 12-well plate. Seed each well with 2 mLs of lactate-purified iPSC-CMs in RPMI 1640 + B27 + insulin and Rock Inhibitor at a density of 1.6 million cells per mL (about 9143 cells/mm^2). Seeding media may be supplemented with 3 μg of Poly-L-Lysine to promote attachment. Allow the cells to grow for a minimum of one week prior to harvesting, using pre-warmed media when washing or feeding. When ready to harvest, move cells to the biosafety cabinet to begin dissociation at room temperature (**Fig. 12**). Fifteen minutes at room temperature should be sufficient for the sheet to dissociate, though supplementing the media with 20 mM HEPES can be used for longer dissociation times.

Using either a serological pipet or a P1000 micropipette, very gently resuspend the cell sheet, starting at the edges and allowing water to enter between the well surface and the cells. Once fully detached, use forceps or the pipette to transfer the cell sheet onto a 1 mm thick glass slide for imaging on the Leica SP8 Confocal Microscope. Ensure the sheet is as flat as possible and in a large drop of media to prevent drying out during the imaging process.

Acknowledgments

Thank you to the Davis lab members, Mack lab members Saffie Mohran, Christian Mandrycky, and Cecelia Watson, and Dale Hailey from the Institute for Stem Cell & Regenerative Medicine and Garvey Imaging Core. Parts of this project received funding from the Mary Gates Endowment for Students and NHLBI Grant R01 HL142624. Fluorescent spectra images were taken from fpbase.org and other figures were created with BioRender.com.

Figures

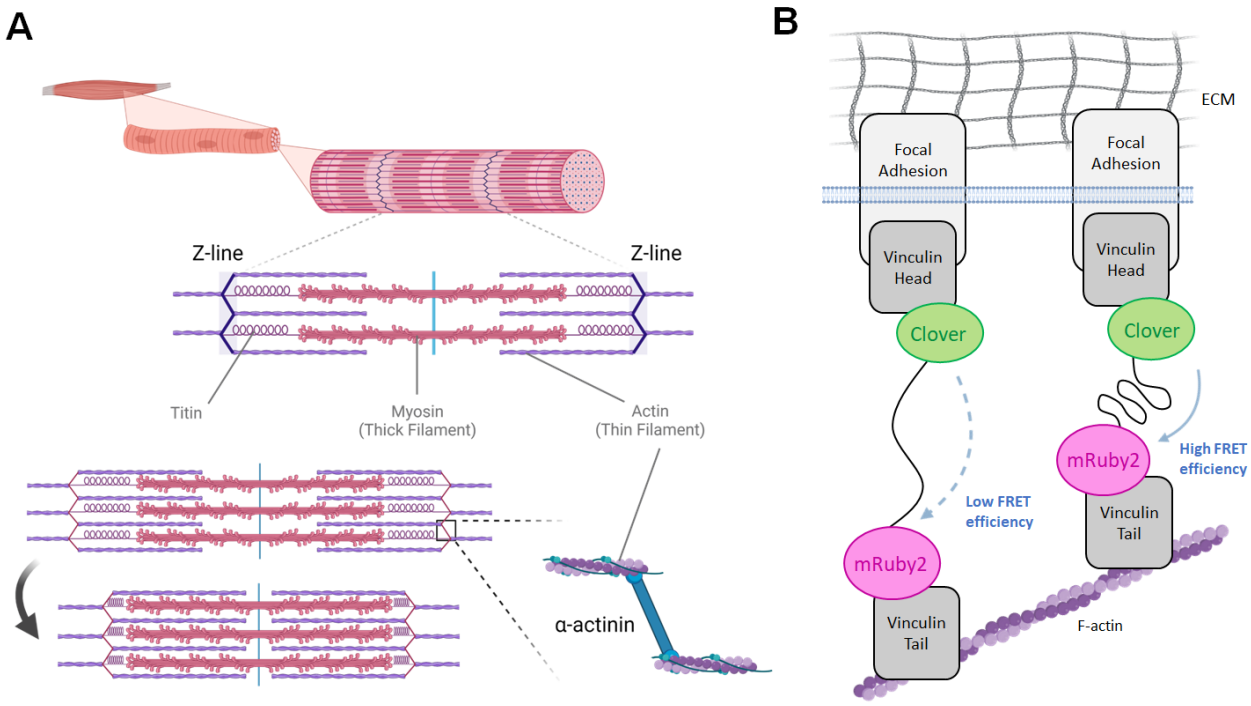

Figure 1. Sarcomere structure and vinculin tension sensor. (A) Sarcomeres are the basic contractile units in muscle cells. When they contract, the thick and thin filaments slide across each other. One of the proteins on the z-line is α-actinin, which binds two actin filaments. (B) The focal adhesion is a transmembrane protein complex. Vinculin is bound to actin which in turn links to sarcomeres. The FRET efficiency of the VinTS depends on the distance between fluorophores. If vinculin is under tension, then the distance between the head and tail of vinculin increases resulting in a decrease in FRET efficiency.

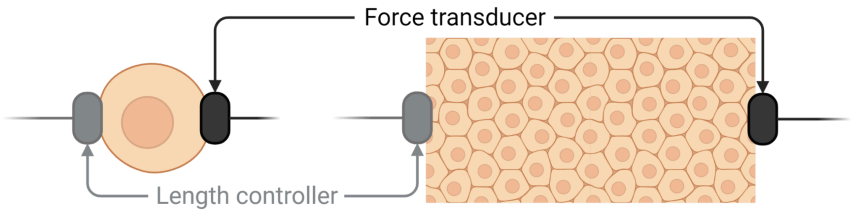

Figure 2. Mechanical rigs for measuring focal adhesion tension would require a multicellular structure. For a single-cell setup, the length controller and force transducer would be placed directly onto the cell membrane, which is where the focal adhesions are located. Alternatively, in a multicellular structure, the two devices can be placed on either end of the tissue and still have many cell-cell contacts with focal adhesions undisturbed by the attachment that can be analyzed.

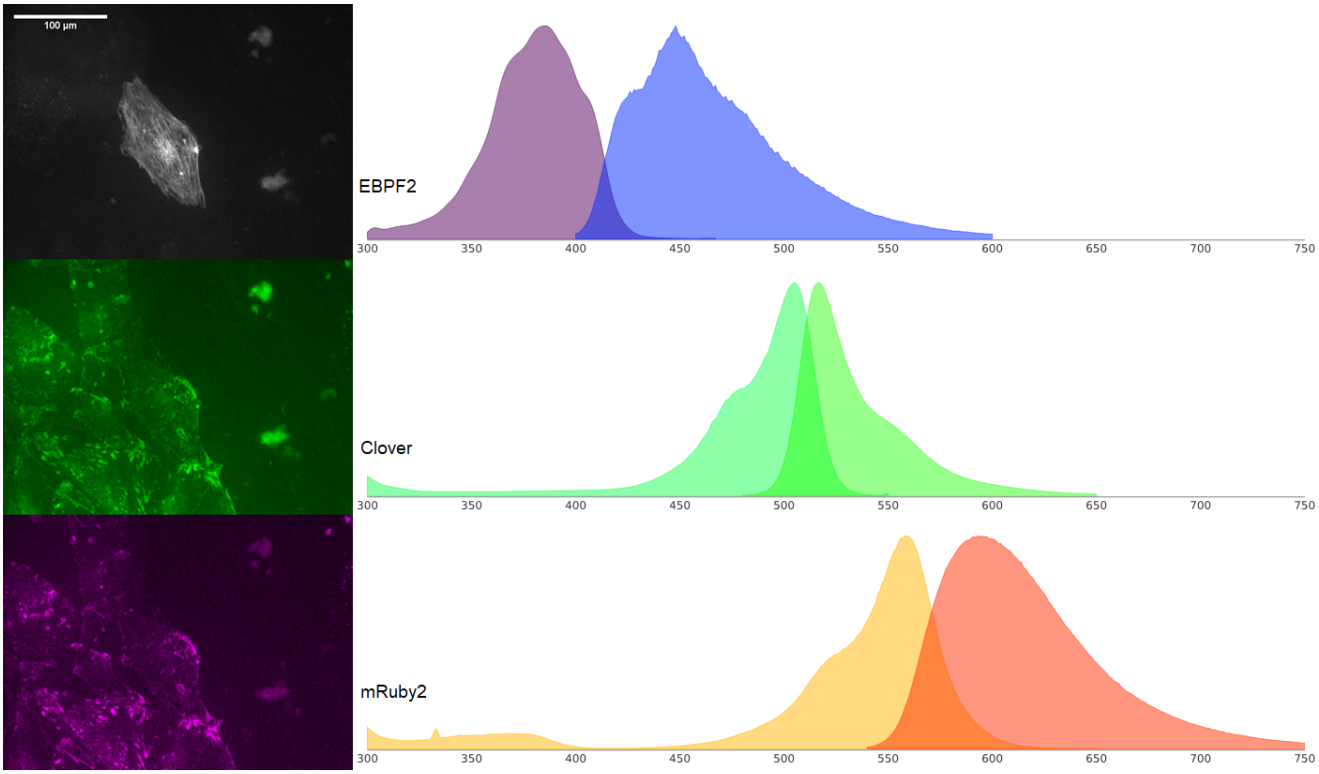

Figure 3. BFP and VinTS expressed in iPSC-CMs. Cellular expression of the fluorophore (left) alongside fluorescent spectra (right) for the BFP (top), Clover (middle), and mRuby2 (bottom). Note how the emission spectra of Clover overlaps with the excitation spectra of mRuby2. Scale bar reads 100 µm.

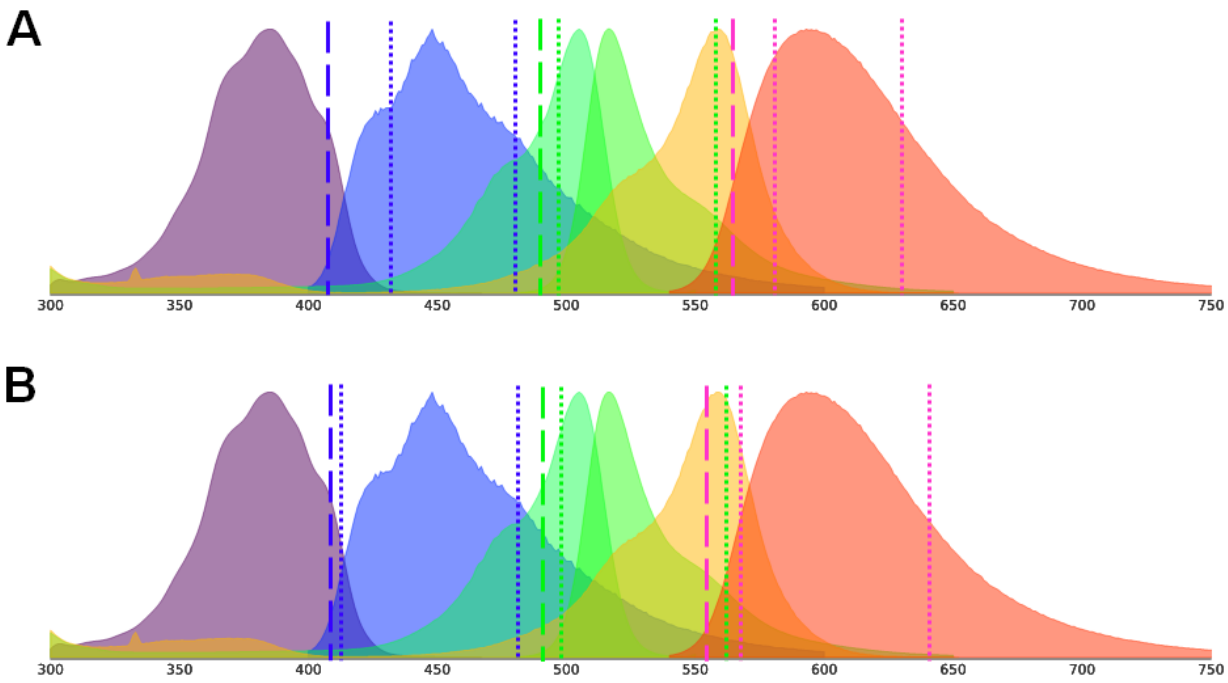

Figure 4. Excitation lasers and collected emission ranges for the Nikon Spinning Disk and Leica Confocal overlaid on the fluorescent spectra of the fluorophores. Dashed lines indicate the excitation wavelength and dotted lines define the range of collected emissions, with the Nikon Spinning Disk Confocal settings on top (A) and Leica SP8 Confocal below (B). The excitation laser and collected wavelengths are as follows for (A) BFP: 405 nm and 430-480 nm, Clover: 488 nm and 495-555 nm, mRuby2: 561 nm and 579-631 nm, and for (B) BFP: 405 nm and 410-480 nm, Clover: 488 nm and 495-560 nm, mRuby2: 552 nm and 565-640 nm.

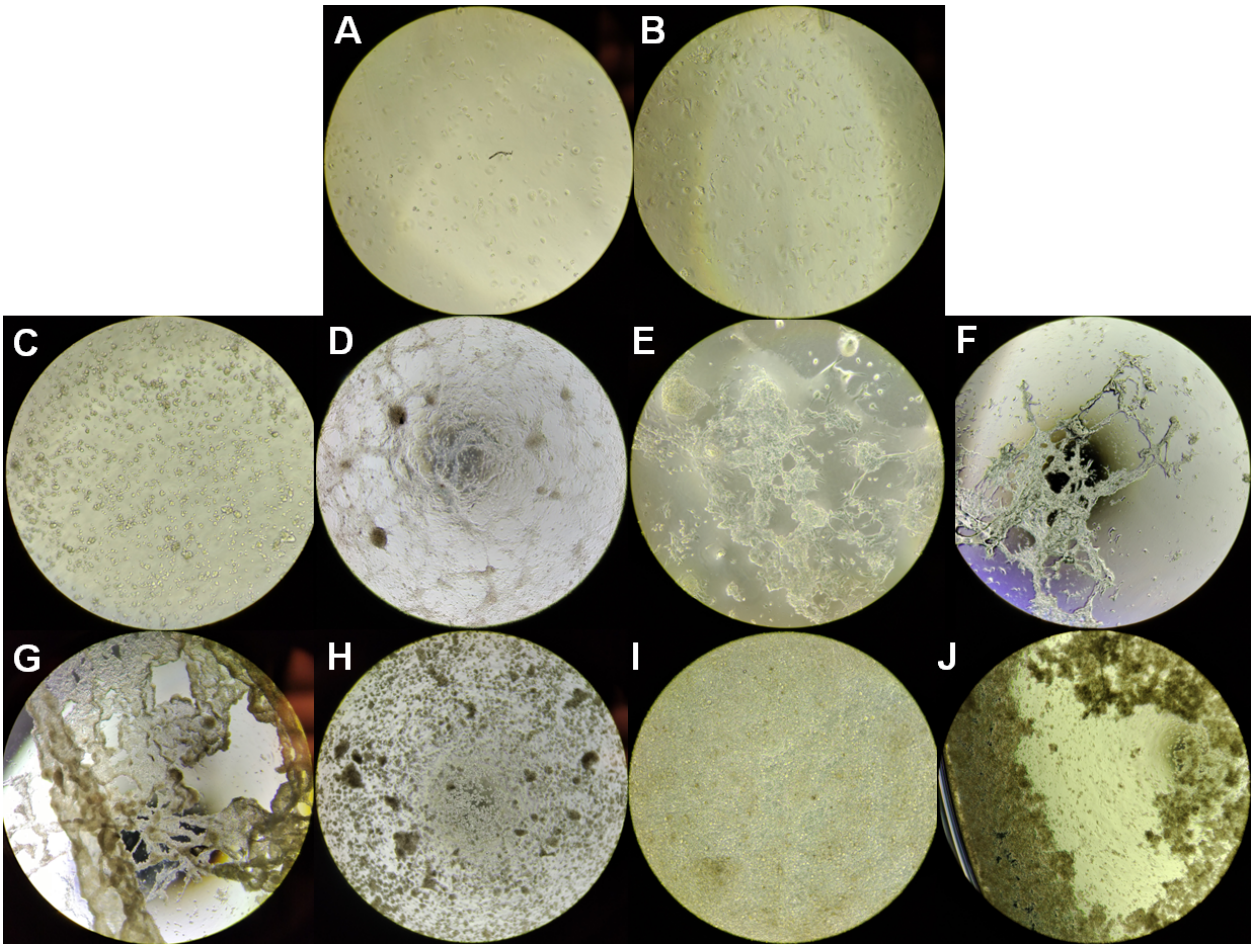

Figure 5. Culturing cardiomyocytes on UpCell™ plates and Cytostretcher chamber wells. These images are taken through the eyepiece of a microscope at 20X magnification of Cytostretcher wells (A-B) and UpCell™ plates (C-J). Representative image of 62k cells/mL (A) and 620k cells/mL seeding density (B). Representative image of an 800k cells/mL seeding density (C), at 2 weeks directly before the dissociation process (D) and after 1.5hrs at room temperature (G). Using membranes to harvest the sheets left many cells and other residue on the surface (E-F). Representative image of a 1600k cells/mL seeding density (H) and one day after seeding (I). Patches of cells have dissociated, leaving gaps in the sheet (J).

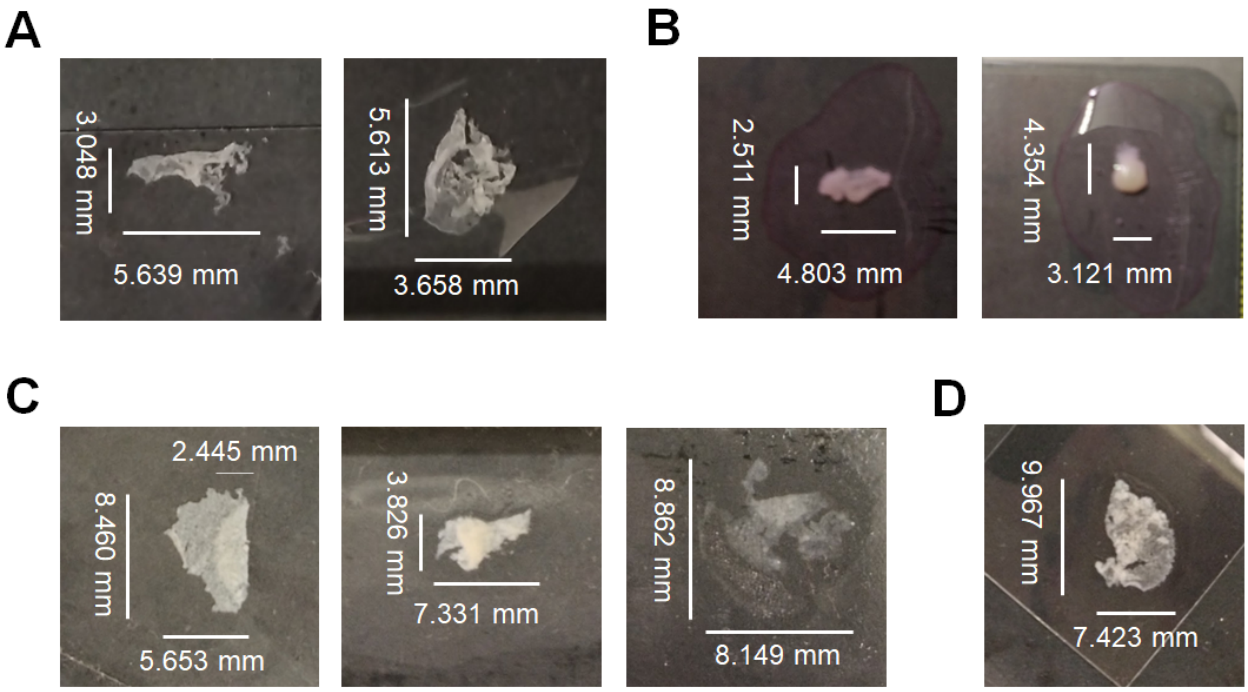

Figure 6. Cell sheets with different seeding and harvesting conditions. Measurements were made using ImageJ. The Batch letter and conditions are as follows: (A) Batch B: 800k/mL, Matrigel, PLL, forceps; (B) Batch F: 1600k/mL, Matrigel, pipettes; (C) Batch C: 1600k/mL, Matrigel, unpurified cells, forceps; (D) Batch H: 1600k/mL, Matrigel, PLL, 10% HS27A, P1000.

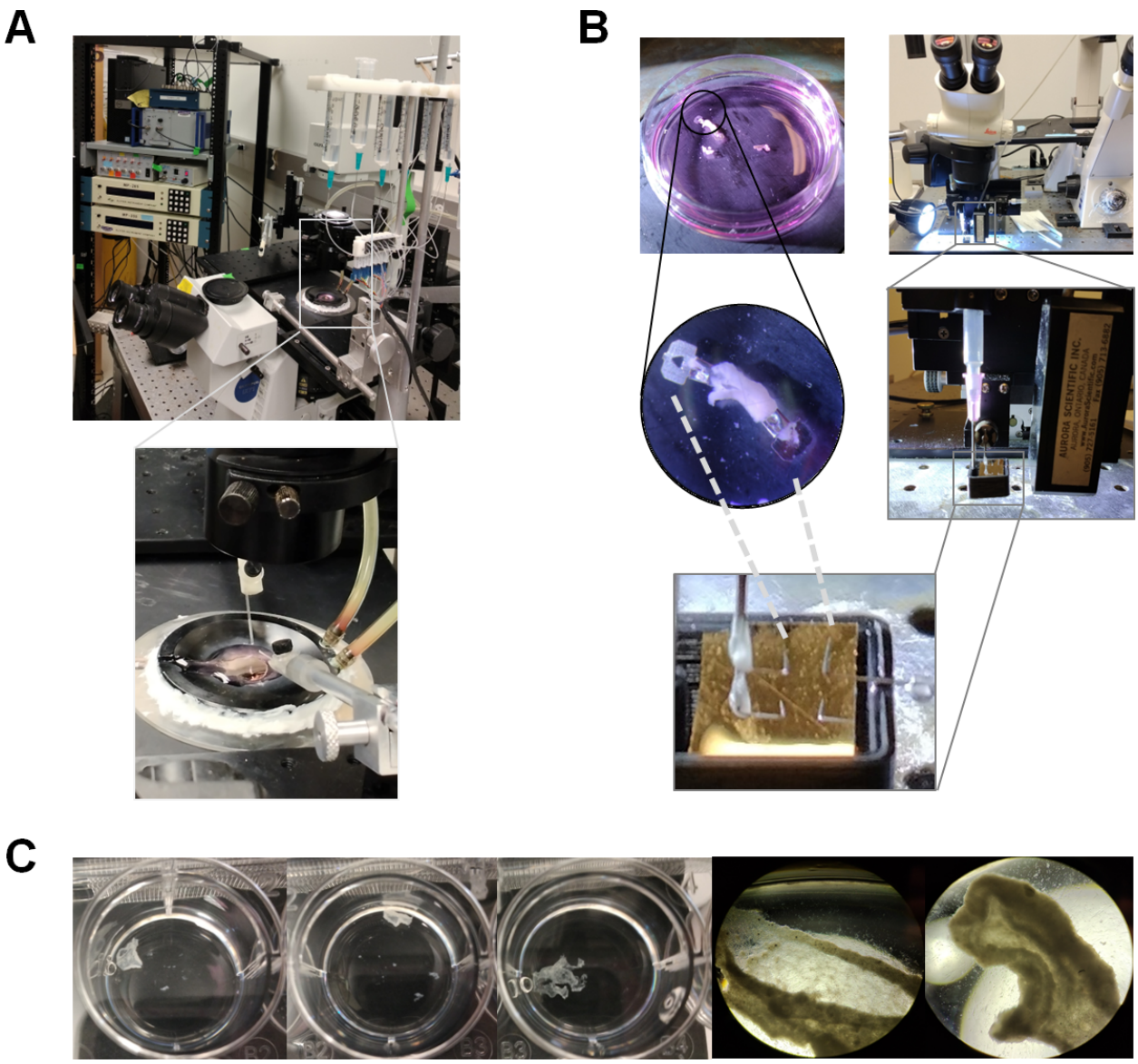

Figure 7. Imaging cell sheets using mechanical rigs adapted to study tension in muscle tissues. (A) Myofibril rig set up with a close-up of the dish. Two glass capillary rods are used to apply strain to the tissue, which is suspended in a well of media. (B) One cell sheet in a 35 mm dish with T-clips attached. The T-clips have holes to hook onto two prongs for force deflection measurements in the intact rig. (C) Three cell sheets in total were harvested for testing the mechanical rig. The third cell sheet was not used in these experiments. The last two close-ups are microscope images taken at 20X magnification of the first two sheets in the series.

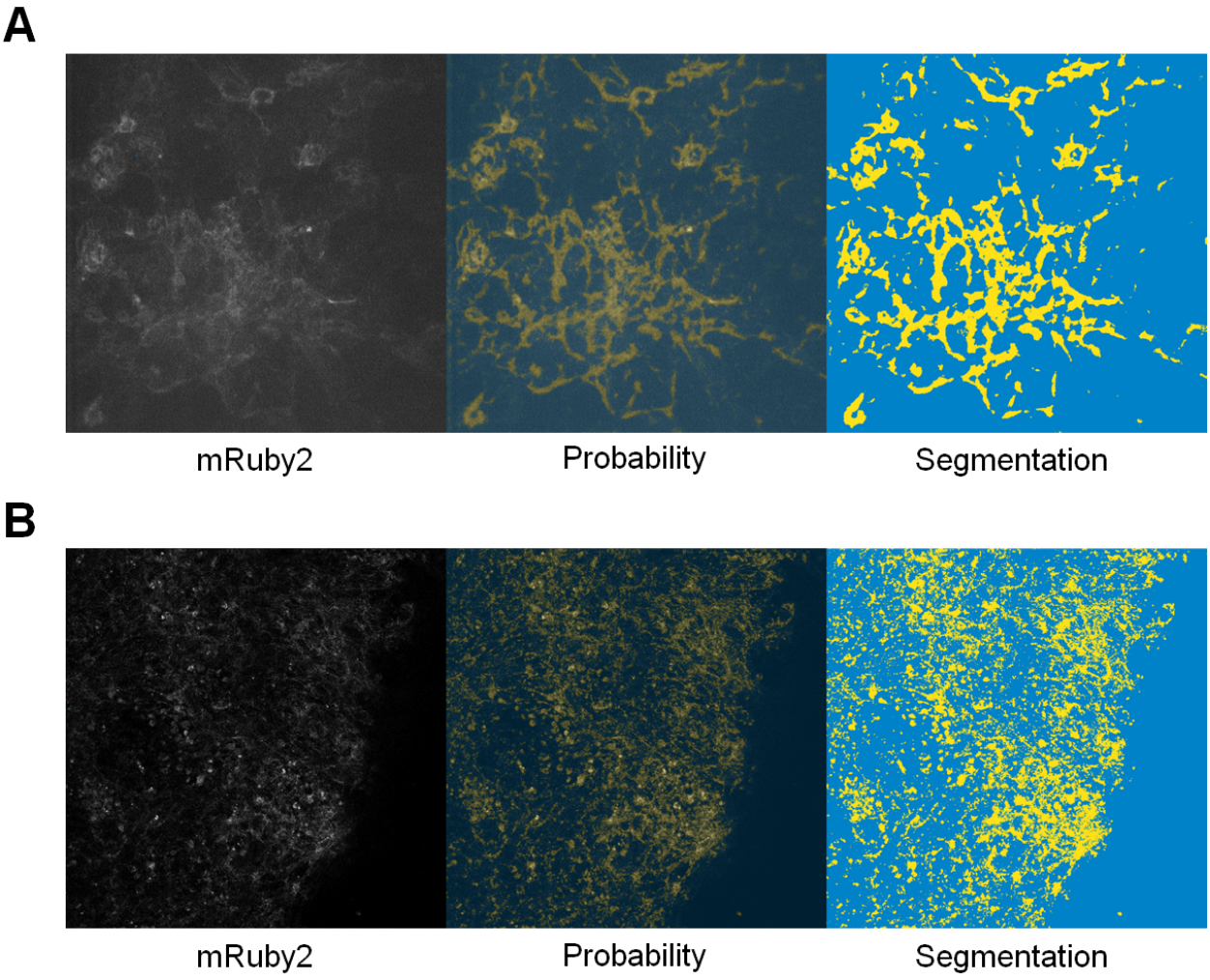

Figure 8. Sample images of the ilastik segmentation process. mRuby2 image (left), probability overlay (center), and binarized segmented pixels (right) for (A) cells cultured on Cytostretcher wells and (B) harvested cell sheets.

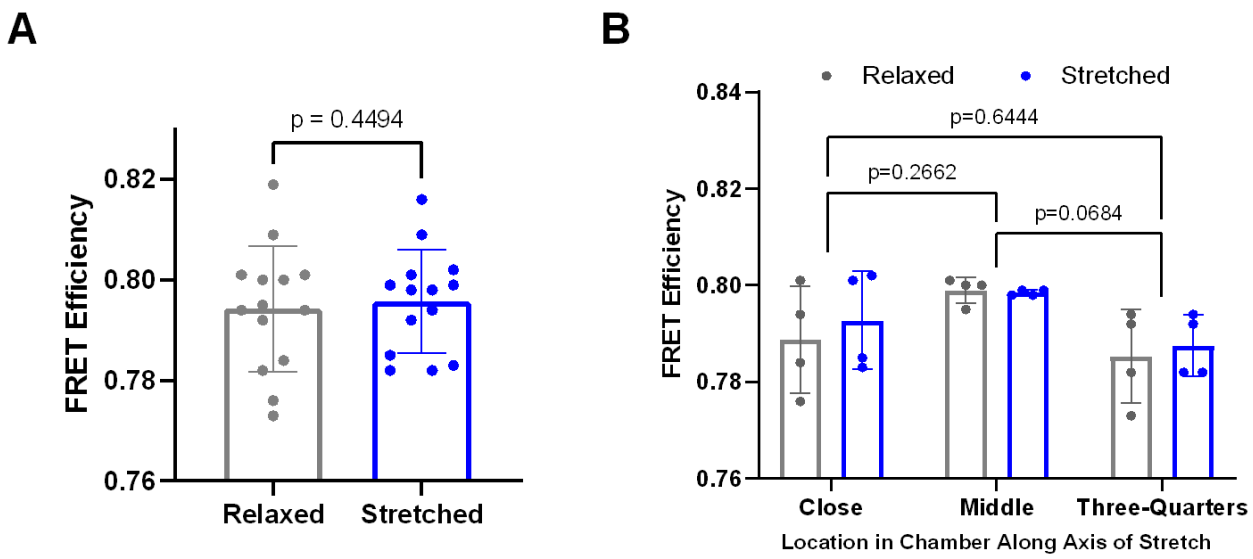

Figure 9. FRET Efficiency of relaxed and stretched cells. (A) FRET efficiency of cells when they are relaxed versus stretched. The average FRET efficiency for the relaxed state was 0.7943 and 0.7957 for the stretched state, with n=14 fields of view from 2 preparations and p=0.4494 by a two-tailed paired t-test. (B) FRET efficiency by location along the stretching axis within the chamber. For the "close", "middle", and "three-quarters" locations respectively, the relaxed and stretched averages are 0.7888 and 0.7928, 0.7990 and 0.7985, and 0.7853 and 0.7875. n=4 for each subgroup and none of the differences between the average of each location group was found to be significant by 2-way ANOVA. The difference between the relaxed averages of each location group and the difference between the stretched averages of each location group was not significant.

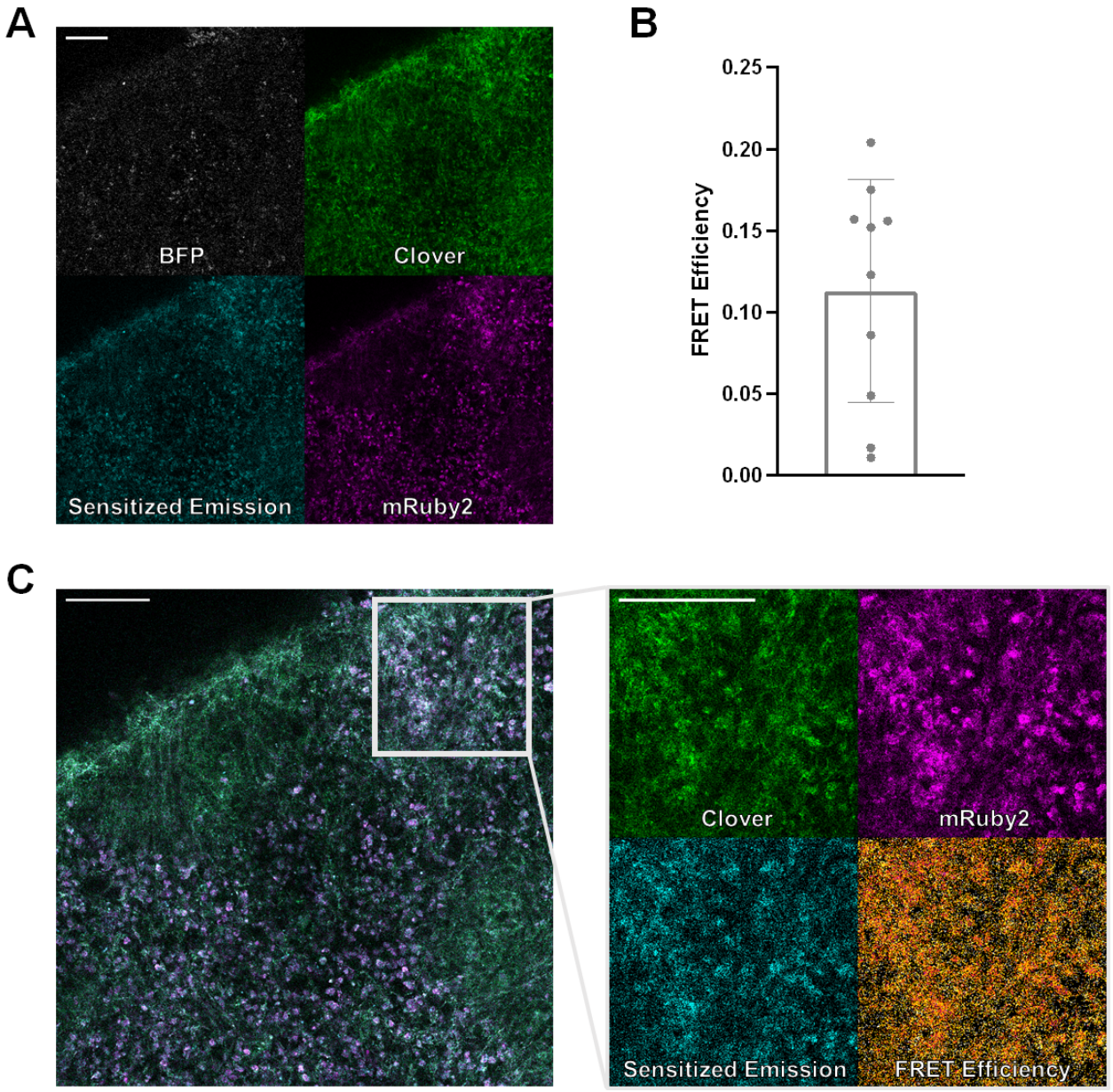

Figure 10. Cell sheets imaged with the Leica SP8 Confocal. (A) Clockwise from top left: BFP, Clover, mRuby2, and sensitized emission fluorescence in a cell sheet. Scale bar reads 100 µm. (B) FRET efficiency of the cell sheets, with an average FRET efficiency of 0.113 and n=10 fields of view. (C) Composite image of the three channels Clover, mRuby2, and sensitized emission. Zoomed callout shows the three channels separately, with a fourth image showing the FRET efficiency.

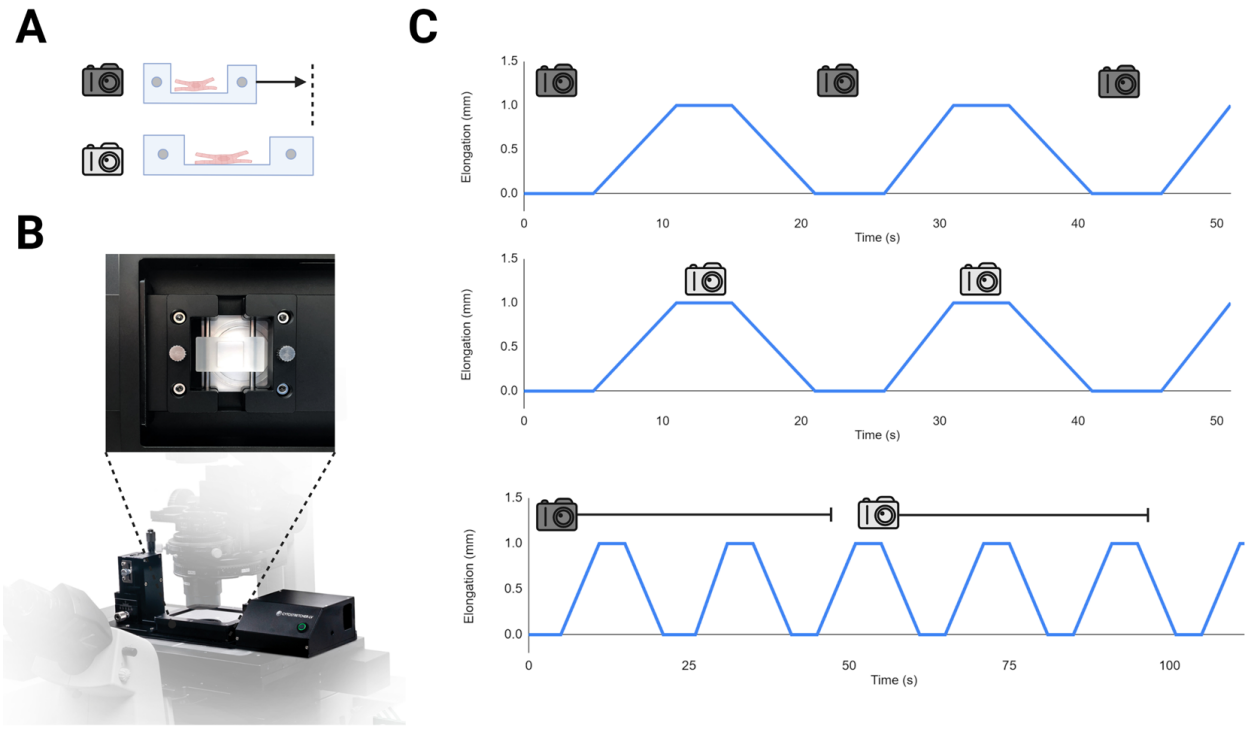

Figure 11. Cytostretcher imaging setup. The dark-colored camera icon denotes images taken when the camera focus is at the relaxed position, and the light-colored camera icon denotes images taken when the camera focus is at the stretched position. (A) Side view of the cells on the cytostretcher chamber when relaxed and when stretched. (B) Top-view close-up of Cytostretcher chamber in the microscope-mountable Cytostretcher-LV. (C) The NaOMI stretching protocol that was used while imaging. The protocol was run once for images taken at the relaxed focus (top), again for the stretched focus (middle), and once more over a longer period of time to take a movie at each focus (bottom).

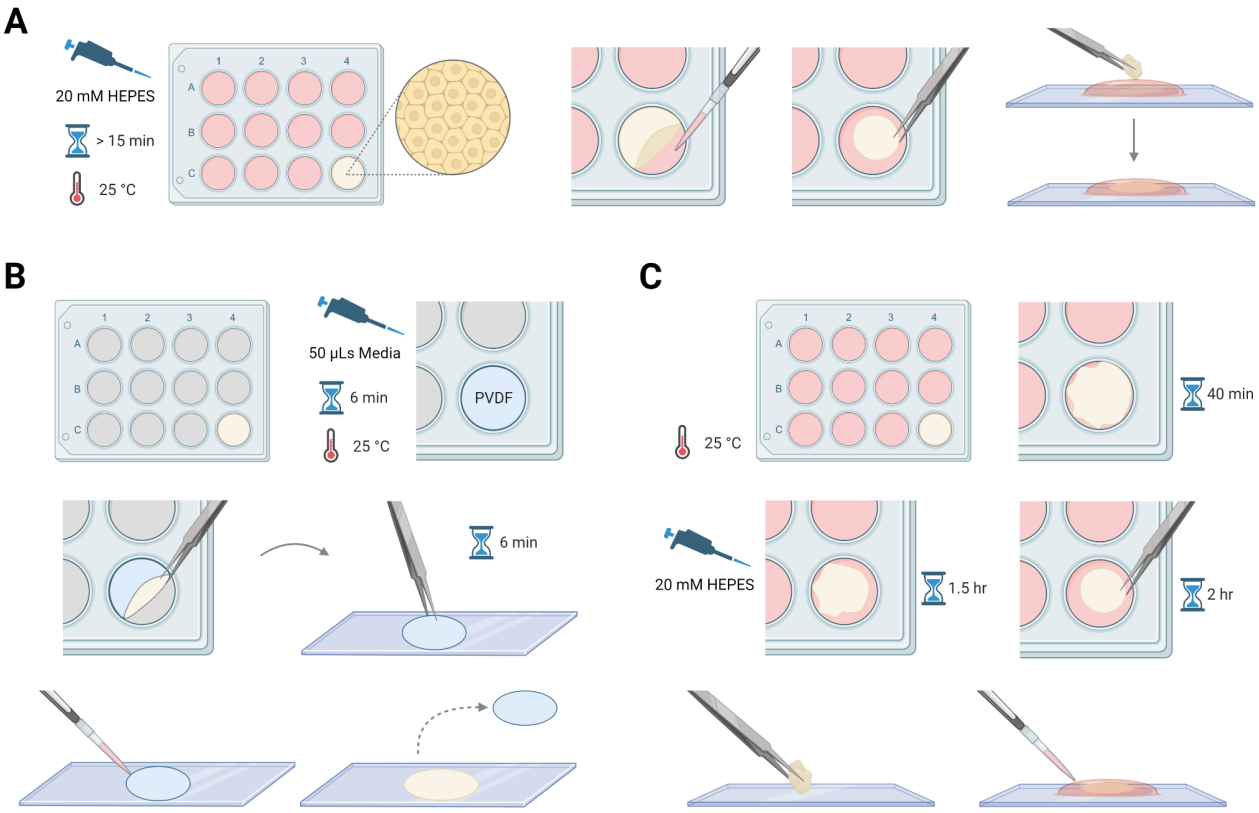

Figure 12. Methods used to harvest cell sheets. Only one well is illustrated, though many wells containing confluent sheets may be cultured at a given time. (A) The most effective method used during harvesting. The 12-well plate is placed at room temperature, supplemented with 20 mM HEPES into the existing media. After 15 minutes, sheets are pipetted off the surface and transferred onto a 1mm glass slide using forceps. (B) The initial method used for harvesting included using a membrane. The plate is placed supernatant is aspirated and 50 µLs of media is added before a PVDF membrane is applied to the top of the sheet. After 6 minutes, the membrane (with cells attached) is peeled from the well and placed with the cells face-down onto a 1 mm glass slide. After another 6 minutes, a small amount of media is added to loosen the membrane away from the cells, leaving only the cells on the glass slide. (C) Another alternate method of harvesting used only forceps. The plate was set out at room temperature, and dissociation from the sides of the well was visible at 40 mins. At 1.5 hours, 20 mM HEPES was added to supplement the media and was nearly all dissociated. At 2 hours, the sheet had dissociated and could be transferred onto a glass slide. A small amount of media is added to allow the sheet to flatten out and prevent it from drying out.

Tables

Batch	Seeding Density (Cells/mL)	Coating & Seeding Conditions	Harvesting Method	Sheets Quality
A 17 days	800k (4 wells total)	Matrigel (4 wells) PLL supplement (1 well) Laminin (1 well)	Membrane & forceps	No sheets (too sparse)
B 15 days	800k (4 wells total)	Matrigel (4 wells) PLL supplement (2 wells)	Membrane, Forceps 20mM HEPES at 1.5hrs	Patchy, two of four successful harvests (**Fig. 6A**)
C 14 days	1600k (4 wells total)	Matrigel	Serological pipette P1000 20mM HEPES	Three of four sheets survived (**Fig. 6C**)
D 18 days	1650k (2 wells total)	Matrigel PLL	P1000 20mM HEPES	Spontaneously dissociated prior to harvest, dense but intact
E -	1600k (2 wells total)	Matrigel (Previously aspirated Matrigel) Unpurified cells	-	Did not attach well Aspirated prior to harvesting
F 17 days	1600k (2 wells total)	Matrigel Unpurified cells	Forceps 20mM HEPES	Dissociated and dense *transfected with BFP (**Fig. 6B**)
G 28 days	1600k (2 wells total)	Matrigel (overnight) PLL 10% HS27A	P1000 20mM HEPES	Partially dissociated prior to harvest, imaged on myofibril and intact rigs (**Fig. 7**)
H 12 days	1600k (1 well total)	Matrigel PLL 10% HS27A	P1000 20mM HEPES	Patches dissociated but intact (**Fig. 6D**)

Table 1. Different seeding and harvesting conditions for cell sheets. Initial attempts were seeded at 800k cells/mL prior to switching to 1600k/mL as the new standard. All wells were pre-coated with Matrigel, with the option of adding either PLL or laminin to supplement. Stromal cell populations of unpurified differentiated cardiomyocytes or 10% HS27A cells was introduced to provide support for the sheets.

Microscope	Capabilities	Limitations
Leica SP8 Confocal	High-resolution imaging up to 60X magnification Quick acquisition of multi-channel images	Not compatible with live-cell imaging using Cytostretcher-LV
Nikon Live-Cell Spinning Disk Confocal	Compatible with live-cell imaging using Cytostretcher-LV Multichannel fluorescent imaging	Magnification limited to 40X objective Not compatible with simultaneous multichannel video acquisition Focus coordinates cannot be changed once acquisition program begins
Myofibril Rig	Precise force measurements for small tissues Fluorescent imaging	Unknown force applied for larger tissues
Intact Rig	Known force measurements for muscle tissues	Not equipped for fluorescent imaging

Table 2. Summary of microscope capabilities and limitations. The Leica Confocal was used to image cell sheets, and the Nikon Spinning Disk was used to conduct stretching experiments using the Cytostretcher-LV. The myofibril rig and intact rig developed in the Mack and Reginer labs were used for stretching cell sheets.

References

[1] I. Kehat and J. D. Molkentin, “Molecular Pathways Underlying Cardiac Remodeling During Pathophysiological Stimulation,” *Circulation*, vol. 122, no. 25, pp. 2727–2735, Dec. 2010, doi: 10.1161/CIRCULATIONAHA.110.942268.

[2] Y.-H. Lin, J. Li, E. R. Swanson, and B. Russell, “CapZ and actin capping dynamics increase in myocytes after a bout of exercise and abates in hours after stimulation ends,” *J. Appl. Physiol.*, vol. 114, no. 11, pp. 1603–1609, Jun. 2013, doi: 10.1152/japplphysiol.01283.2012.

[3] K. M. Wisdom, S. L. Delp, and E. Kuhl, “Use it or lose it: multiscale skeletal muscle adaptation to mechanical stimuli”, *Biomech Model Mechanobiol*, vol. 14, pp. 195–215, Sep. 2014, doi: 10.1007/s10237-014-0607-3.

[4] P. S. Azevedo, B. F. Polegato, M. F. Minicucci, S. A. R. Paiva, and L. A. M. Zornoff, “Cardiac Remodeling: Concepts, Clinical Impact, Pathophysiological Mechanisms and Pharmacologic Treatment,” *Arq. Bras. Cardiol.*, vol. 106, no. 1, pp. 62–69, Jan. 2016, doi: 10.5935/abc.20160005.

[5] L. Schirone *et al.*, “A Review of the Molecular Mechanisms Underlying the Development and Progression of Cardiac Remodeling,” *Oxid. Med. Cell. Longev.*, vol. 2017, p. 3920195, 2017, doi: 10.1155/2017/3920195.

[6] C. O’Mahony, P. Elliott, and W. McKenna, “Sudden Cardiac Death in Hypertrophic Cardiomyopathy,” *Circ. Arrhythm. Electrophysiol.*, vol. 6, no. 2, pp. 443–451, Apr. 2013, doi: 10.1161/CIRCEP.111.962043.

[7] J. T. Pearson *et al.*, “Effects of Sustained Length-Dependent Activation on In Situ Cross-Bridge Dynamics in Rat Hearts,” *Biophys. J.*, vol. 93, no. 12, pp. 4319–4329, Dec. 2007, doi: 10.1529/biophysj.107.111740.

[8] C.-G. Lim, J. Jang, and C. Kim, “Cellular machinery for sensing mechanical force,” *BMB Rep.*, vol. 51, no. 12, pp. 623–629, Dec. 2018, doi: 10.5483/BMBRep.2018.51.12.237.

[9] D. W. Dumbauld *et al.*, “How vinculin regulates force transmission,” *Proc. Natl. Acad. Sci.*, vol. 110, no. 24, pp. 9788–9793, Jun. 2013, doi: 10.1073/pnas.1216209110.

[10] J. D. Humphries, P. Wang, C. Streuli, B. Geiger, M. J. Humphries, and C. Ballestrem, “Vinculin controls focal adhesion formation by direct interactions with talin and actin,” *J. Cell Biol.*, vol. 179, no. 5, pp. 1043–1057, Dec. 2007, doi: 10.1083/jcb.200703036.

[11] P. Pandey *et al.*, “Cardiomyocytes Sense Matrix Rigidity through a Combination of Muscle and Non-muscle Myosin Contractions,” *Dev. Cell*, vol. 44, no. 3, pp. 326-336.e3, Feb. 2018, doi: 10.1016/j.devcel.2017.12.024.

[12] J. Davis *et al.*, “A Tension-Based Model Distinguishes Hypertrophic versus Dilated Cardiomyopathy,” *Cell*, vol. 165, no. 5, pp. 1147–1159, May 2016, doi: 10.1016/j.cell.2016.04.002.

[13] J. Zhao, F. Meng, J. Qian, Y. Huang, and Y. Fan, “In vitro cell stretching devices and their applications: From cardiomyogenic differentiation to tissue engineering,” *Med. Nov. Technol. Devices*, vol. 18, p. 100220, Jun. 2023, doi: 10.1016/j.medntd.2023.100220.

[14] A. Chopra *et al.*, “Force Generation via β-Cardiac Myosin, Titin, and α-Actinin Drives Cardiac Sarcomere Assembly from Cell-Matrix Adhesions,” *Dev. Cell*, vol. 44, no. 1, pp. 87-96.e5, Jan. 2018, doi: 10.1016/j.devcel.2017.12.012.

[15] O. Campàs *et al.*, “Quantifying cell-generated mechanical forces within living embryonic tissues,” *Nat. Methods*, vol. 11, no. 2, pp. 183–189, Feb. 2014, doi: 10.1038/nmeth.2761.

[16] G. Bartalena, R. Grieder, R. I. Sharma, T. Zambelli, R. Muff, and J. G. Snedeker, “A novel method for assessing adherent single-cell stiffness in tension: design and testing of a substrate-based live cell functional imaging device,” *Biomed. Microdevices*, vol. 13, no. 2, pp. 291–301, Apr. 2011, doi: 10.1007/s10544-010-9493-3.

[17] G. Rápalo, J. D. Herwig, R. Hewitt, K. R. Wilhelm, C. M. Waters, and E. Roan, “Live Cell Imaging during Mechanical Stretch,” *JoVE J. Vis. Exp.*, no. 102, p. e52737, Aug. 2015, doi: 10.3791/52737.

[18] B. D. Riehl, J.-H. Park, I. K. Kwon, and J. Y. Lim, “Mechanical Stretching for Tissue Engineering: Two-Dimensional and Three-Dimensional Constructs,” *Tissue Eng. Part B Rev.*, vol. 18, no. 4, pp. 288–300, Aug. 2012, doi: 10.1089/ten.teb.2011.0465.

[19] V. Du *et al.*, “A 3D magnetic tissue stretcher for remote mechanical control of embryonic stem cell differentiation,” *Nat. Commun.*, vol. 8, no. 1, Art. no. 1, Sep. 2017, doi: 10.1038/s41467-017-00543-2.

[20] K. C. Neuman and A. Nagy, “Single-molecule force spectroscopy: optical tweezers, magnetic tweezers and atomic force microscopy,” *Nat. Methods*, vol. 5, no. 6, pp. 491–505, Jun. 2008, doi: 10.1038/nmeth.1218.

[21] A.-L. Cost, P. Ringer, A. Chrostek-Grashoff, and C. Grashoff, “How to Measure Molecular Forces in Cells: A Guide to Evaluating Genetically-Encoded FRET-Based Tension Sensors,” *Cell. Mol. Bioeng.*, vol. 8, no. 1, pp. 96–105, Dec. 2014, doi: 10.1007/s12195-014-0368-1.

[22] Z. Tang and T. Okano, “Recent development of temperature-responsive surfaces and their application for cell sheet engineering,” *Regen. Biomater.*, vol. 1, no. 1, pp. 91–102, Nov. 2014, doi: 10.1093/rb/rbu011.

[23] A. J. Lam *et al.*, “Improving FRET dynamic range with bright green and red fluorescent proteins,” *Nat. Methods*, vol. 9, no. 10, pp. 1005–1012, Oct. 2012, doi: 10.1038/nmeth.2171.

[24] Nature Education, “poly-A tail,” *Scitable*, 2014. https://www.nature.com/scitable/definition/poly-a-tail-276/.

[25] “ibidi Stage Top Incubator | CO2 Regulation | Universal Fit,” *ibidi*. https://ibidi.com/stage-top-incubators/230-ibidi-stage-top-incubation-system-universal-fit-f

or-1-chamber-co2.html.

[26] “Cytostretcher,” *Curi Bio*. https://www.curibio.com/cytostretcher.

[27] “Thermo Scientific Nunc Temperature-Responsive Cell Culture Surface | Thermo Fisher Scientific - US.” https://www.thermofisher.com/us/en/home/life-science/cell-culture/cell-culture-plastics/temperature-responsive-cell-culture-surface.html.

[28] “Medium Cytostretcher Chamber,” *Curi Bio*. https://www.curibio.com/products/cs-0144.

[29] “DFU PhotoGel with irgacure 5215 Methacrylated Gelatin Rev 03.pdf.” [Online]. Available: https://advancedbiomatrix.com/public/pdf/DFU%20PhotoGel%20with%20irgacure%205215%20Methacrylated%20Gelatin%20Rev%2003.pdf

[30] fret-analysis group. (2018) fret-analysis [Computer Software]. GitLab. Retrieved Sep. 21, 2022 from https://gitlab.oit.duke.edu/HoffmanLab-Public